

Empirical Line Lists in the ExoMol Database

Yixin Wang, Jonathan Tennyson *  and Sergei N. Yurchenko 

Department of Physics and Astronomy, University College London, London WC1E 6BT, UK; wyx7201@mail.nankai.edu.cn (Y.W.); s.yurchenko@ucl.ac.uk (S.N.Y.)

* Correspondence: j.tennyson@ucl.ac.uk

Received: 20 December 2019; Accepted: 11 February 2020; Published: 17 February 2020



Abstract: The ExoMol database aims to provide comprehensive molecular line lists for exoplanetary and other hot atmospheres. The data are expanded by inclusion of empirically derived line lists taken from the literature for a series of diatomic molecules, namely CH, NH, OH, AlCl, AlF, OH⁺, CaF, MgF, KF, NaF, LiCl, LiF, MgH, TiH, CrH, FeH, C₂, CP, CN, CaH, and triplet N₂. Generally, these line lists are constructed from measured spectra using a combination of effective rotational Hamiltonian models for the line positions and ab initio (transition) dipole moments to provide intensities. This work results in the inclusion of 22 new molecules (36 new isotopologues) in the ExoMol database.

Keywords: astronomical data bases; Exoplanets; brown stars; cool stars; opacity; molecular spectra; ExoMol

1. Introduction

The ExoMol project [1] aims to provide comprehensive spectroscopic data for molecules which are important for exoplanetary and other hot astronomical atmospheres. Thus far, these data have been provided in the form of computed line lists generated as part of the ExoMol project itself or taken from other sources which use a similar methodology. In principle, it is possible to compute line lists by a direct numerical solution of the appropriate Schrödinger equation and the procedure for doing this, which involves initially using the Born–Oppenheimer approximation to separate the electronic and nuclear motion, is now well-established [2]. However, while there are a number of codes available [3] which can provide accurate solutions to the few-body nuclear motion problem using the variational principle, it is generally not possible to solve the electronic structure problem with the required accuracy for most molecules of interest; see [4] for a discussion of some of the issues involved.

The ExoMol project has therefore used a methodology [5,6] which involves the construction of an appropriate spectroscopic model based on a combination of ab initio potential energy curves (PECs), dipole moment functions (DMFs) and, where appropriate, coupling curves. It is found that, with the use of appropriate electronic structure methods, ab initio dipole moment surfaces can provide reliable transition intensities [7] even with quantified uncertainties if these are needed [8]. However, to obtain accurate transition frequencies, the ab initio potential energy surfaces (or curves for diatomic molecules) need to be refined using experimental data; see [9] for a discussion of the procedure used. For open shell systems, various angular momenta, spin-orbit, spin-rotation, etc. interactions can couple the potential energy curves; see [10]. These couplings may also be refined. We have developed a suite of programs for this task [3,11] based on a variational solution of the nuclear Schrödinger equation. The final problem solved using these programs, and the programs themselves, can be referred to as the spectroscopic model used to characterize the particular line list. Provision of this model ensures not only that the results are reproducible, but also allows results to be improved or extended using the model as a starting point. Indeed, post hoc improvement of our line lists is an important part of our general procedure; see [12], for example.

The current data base (www.exomol.com [13]) contains line lists for some 60 molecules generated in this fashion. In many cases, there are corresponding line lists for isotopically substituted species. A number of the ExoMol line lists contain many billions of transitions.

However, line lists can be generated directly using laboratory measurements [14]. While these line lists are rarely as complete (or as large) as computed ones, they can be significantly more accurate, particularly in the line positions. These measurements can also provide data on systems for which computed line lists are presently unavailable, or indeed, in some cases, they would be very difficult to construct. It is therefore useful to augment the current ExoMol database with appropriate empirical line lists. The purpose of this article is to report progress in doing just that.

In practice, the methodology used to construct the computed and empirical line lists can be closer than is apparent at first sight. While computed line lists often use experimental data to improve not only the potentials used but also the positions of both whole vibrational bands [15] and individual transitions (eg Barber et al. [12]), as discussed below, the empirical line lists often use dipole moment curves computed ab initio to generate line intensities. In this case, the final line lists may be generated either via effective Hamiltonian fits to the laboratory data, using programs such as PGOPHER [16], or by direct solution of the appropriate nuclear motion Schrödinger equation, for which Le Roy's program LEVEL [17] is often used. Thus, the empirical approach considered here, see [18], also provides a spectroscopic model for each line list.

2. Method

The ExoMol format of line lists assumes two files, a States file (.states) and a Transitions file (.trans). There is one such file for each isotopologue considered. The states file contains term energies (cm^{-1}) and the state description. This description consists of the state's IDs, total statistical weights, total rotational angular momentum J (integer or half-integer), and other quantum numbers (vibrational, rotational, electronic, symmetry, etc.), state lifetimes, and Landé g -factors [19]. An extension to include the uncertainty in the energy will be implemented in the next release of the data base [20]. The transition file contains the upper and lower state IDs, Einstein A coefficients (s^{-1}) and, optionally, transition frequencies (cm^{-1}). As an example, Tables 1 and 2 give extracts from ExoMol States and Transition files for the new ${}^7\text{Li}^{35}\text{Cl}$ line list.

Table 1. Extract from the states file of the ${}^7\text{Li}^{35}\text{Cl}$ line list.

i	Energy (cm^{-1})	g_i	J	τ	v
1	0.000000	16	0	-1.0000E+00	0
2	1.405000	48	1	6.4935E+04	0
3	4.215000	80	2	6.8027E+03	0
4	8.430000	112	3	1.8762E+03	0
5	14.049000	144	4	7.6336E+02	0
6	21.072000	176	5	3.8168E+02	0
7	29.499000	208	6	2.1786E+02	0
8	39.331000	240	7	1.3569E+02	0
9	50.564000	272	8	9.0090E+01	0
10	63.200000	304	9	6.2893E+01	0
11	77.237000	336	10	4.5662E+01	0
12	92.674000	368	11	3.4130E+01	0
13	109.511000	400	12	2.6247E+01	0
14	127.747000	432	13	2.0576E+01	0
15	147.380000	464	14	1.6447E+01	0

i : State counting number; \tilde{E} : State energy in cm^{-1} ; g_i : Total statistical weight, equal to $g_{\text{ns}}(2J + 1)$; J : Total angular momentum; τ : Lifetime (s^{-1}); v : State vibrational quantum number.

Table 2. Extract from the transitions file of the ${}^7\text{Li}{}^{35}\text{Cl}$ line list.

f	i	A_{fi} (s^{-1})	$\tilde{\nu}_{fi}$
492	475	1.1900E+01	110.073000
1381	1370	1.5400E+01	110.207000
951	939	1.3300E+01	110.289000
1190	1178	1.4400E+01	110.386000
859	840	1.3100E+01	110.544000
1323	1313	1.5200E+01	110.605000
1122	1110	1.4200E+01	110.716000
738	721	1.2800E+01	110.780000
1264	1252	1.5000E+01	110.988000
624	606	1.2600E+01	110.997000
1049	1035	1.3900E+01	111.028000
1390	1381	1.5900E+01	111.110000
513	492	1.2300E+01	111.193000

f : Upper state counting number; i : Lower state counting number; A_{fi} : Einstein-A coefficient in s^{-1} ; $\tilde{\nu}_{fi}$: transition wavenumber in cm^{-1} .

Most of the experimental line lists presented in this work were collected from the MoLLIST website <http://bernath.uwaterloo.ca/molecularlists.php> [18], the exception being the N_2 line list which is due to Western et al. [21]. These line lists were then converted to the ExoMol format [13] using the following standard steps: (i) Extract states which correspond to unique sets of quantum numbers and energies and convert into the ExoMol format: all states are labelled with a unique ID which is simply the counting number of the state in the .states file (line number); (ii) Using the state IDs, generate a .trans file in the ExoMol format: ID_f , ID_i , A_{fi} and $\tilde{\nu}_{fi}$. This procedure was used for all species except N_2 , NH and CH . In case of N_2 , the ExoMol format was generated directly from the latest version of PGOPHER [21] using this new PGOPHER feature. For C_2 , CH and NH , the line lists were reformatted by Villanueva et al. [22].

The partition functions were computed using (in most cases) the data by Sauval and Tatum [23] or Barklem and Collet [24], and corrected to be in the “physicists” convention [25], as used by ExoMol and HITRAN [26]; this convention includes the full nuclear spin degeneracy. The lifetimes were generated using the methodology reported by Tennyson et al. [27].

A summary of the empirical line lists (mostly from Bernath’s group) is given in Table 3.

Table 3. Empirical line list included in the ExoMol database. The number of lines and number of states included in each line list are given. The maximal temperatures of the partition functions is $T = 5000$ K. All MoLLIST empirical line lists are named ‘MoLLIST’. The N_2 line list by Western et al. [21] is called ‘WCCRMT’.

Molecule	El. States	ν_{max}	J^{max}	Lines	N States	Ref.
Al^{35}Cl	$X^1\Sigma^+$	11	200	20245	2423	Yousefi and Bernath [28]
Al^{37}Cl	$X^1\Sigma^+$	11	200	20245	2423	Yousefi and Bernath [28]
AlF	$X^1\Sigma^+$	11	200	40490	2423	Yousefi and Bernath [28]
${}^{12}\text{CH}$	$X^2\Pi, A^2\Delta, B^2\Sigma^-, C^2\Sigma^+$	6	49.5	53,079	2526	Masseron et al. [29]
${}^{13}\text{CH}$	$X^2\Pi, A^2\Delta, B^2\Sigma^-, C^2\Sigma^+$	6	49.5	51,349	2428	Masseron et al. [29]
NH	$X^3\Sigma^-, A^3\Pi$	6	45	22,545	1285	Brooke et al. [30,31], Fernando et al. [32]
OH	$X^2\Pi, A^2\Sigma^+$	13	58.5	54,276	1878	Brooke et al. [33], Yousefi et al. [34]
OH^+	$X^3\Sigma^-, A^3\Pi$	4	30	12,044	823	Hodges and Bernath [35], Hodges et al. [36]
${}^{40}\text{CaF}$	$X^2\Sigma^+$	10	123	14,817	1363	Hou and Bernath [37]
${}^{42}\text{CaF}$	$X^2\Sigma^+$	10	123	14,817	1363	Hou and Bernath [37]
${}^{43}\text{CaF}$	$X^2\Sigma^+$	10	123	14,817	1363	Hou and Bernath [37]
${}^{44}\text{CaF}$	$X^2\Sigma^+$	10	123	14,817	1363	Hou and Bernath [37]
${}^{46}\text{CaF}$	$X^2\Sigma^+$	10	123	14,817	1363	Hou and Bernath [37]
${}^{48}\text{CaF}$	$X^2\Sigma^+$	10	123	14,817	1363	Hou and Bernath [37]
${}^{39}\text{KF}$	$X^1\Sigma^+$	10	110	10,572	1065	Frohman et al. [38]
${}^{41}\text{KF}$	$X^1\Sigma^+$	10	109	10,379	1047	Frohman et al. [38]

Table 3. Cont.

Molecule	El. States	v_{\max}	J^{\max}	Lines	N States	Ref.
NaF	$X^1\Sigma^+$	10	90	7884	839	Frohman et al. [38]
^{24}MgF	$X^2\Sigma^+$	8	101	8136	917	Hou and Bernath [39]
^{25}MgF	$X^2\Sigma^+$	8	101	8136	917	Hou and Bernath [39]
^{26}MgF	$X^2\Sigma^+$	8	101	8136	917	Hou and Bernath [39]
$^6\text{Li}^{35}\text{Cl}$	$X^1\Sigma^+$	11	201	26,260	2423	Bittner and Bernath [40]
$^6\text{Li}^{37}\text{Cl}$	$X^1\Sigma^+$	11	201	26,260	2423	Bittner and Bernath [40]
$^7\text{Li}^{35}\text{Cl}$	$X^1\Sigma^+$	11	201	26,260	2423	Bittner and Bernath [40]
$^7\text{Li}^{37}\text{Cl}$	$X^1\Sigma^+$	11	201	26,260	2423	Bittner and Bernath [40]
^6LiF	$X^1\Sigma^+$	11	201	10,621	2423	Bittner and Bernath [40]
^7LiF	$X^1\Sigma^+$	11	201	10,621	2423	Bittner and Bernath [40]
MgH	$X^2\Sigma^+, A^2\Pi, B'^2\Sigma^+$,	11	50.5	30896	1935	GharibNezhad et al. [41]
TiH	$X^4\Phi, A^4\Phi, B^4\Gamma$	5	50.5	199,072	5788	Burrows et al. [42]
CrH	$X^6\Sigma^+, A^6\Sigma^+$	3	39.5	13,824	1646	Chowdhury et al. [43]
FeH	$X^4\Delta, F^4\Delta$	4	50.5	93,040	3564	Wende et al. [44]
C_2	$a^3\Pi_g, d^3\Pi_u$	3	97	155,110	4653	Brooke et al. [45]
CP	$X^2\Sigma^+, A^2\Pi$	8	55.5	28,752	2114	Ram et al. [46]
CN	$X^2\Sigma^+, A^2\Pi, B^2\Sigma^+$	22	115.5	195,120	7703	Brooke et al. [47]
CaH	$X^2\Sigma^+, A^2\Pi, B^2\Sigma^+, E^2\Pi$	4	50.5	19,095	1771	Li et al. [48], Shayesteh et al. [49]
N_2	$A^3\Sigma_u^+, B^3\Pi_g, B'^3\Sigma_u^-, W^3\Delta_u$	29	75	7,182,000	40,380	Western et al. [21]

2.1. AlCl and AlF

Vibrational-rotational line lists for AlCl and AlF in their ground ($X^1\Sigma^+$) electronic states are provided by Yousefi and Bernath [28]. The line lists were generated using experimental high-resolution ro-vibrational and rotational line positions: 1100 AlF transitions by Zhang et al. [50] and 1544 transitions of Al³⁵Cl and Al³⁷Cl by Hedderich et al. [51] were used to obtain empirically the potential energy curves (PECs) by fitting. The PECs were used to calculate ro-vibrational energy levels for the vibrational excitations $v = 0$ to $v = 11$ and up to $J_{\max} = 200$ using program LEVEL [17]. Ab initio dipole moment functions covering the PECs turning points were calculated and used to determine line intensities.

Line lists were converted to ExoMol states and transition files; partition functions up to 5000 K were calculated with the program Exocross [52] using the energies from the line list. The quantum numbers used for these line lists are simply J and v . Sample spectra are shown in Figure 1.

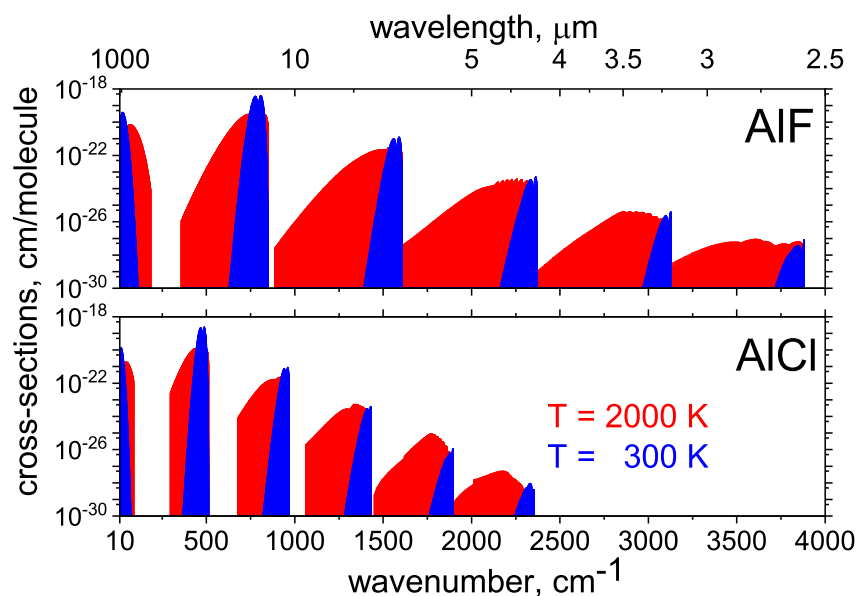


Figure 1. Cross sections of AlCl and AlF computed using the line list by Yousefi and Bernath [28] represented in the ExoMol format.

2.2. CH

The original empirical line list for CH was produced by Masseron et al. [29]. First, PGOPHER was used to determine spectroscopic constants by fitting to the experimental data. The global fit included the following experimental data: the $X^2\Pi$ ro-vibrational fundamental transitions of Colin and Bernath [53] from the ACE (Atmospheric Chemical Experiment); the solar spectrum of Bernath et al. [54]; $A^2\Delta - X^2\Pi$ transitions from the laboratory measurements by Bernath et al. [55] and Zachwieja [56]; $B^2\Sigma^- - X^2\Pi$ transitions due to Kepa et al. [57], Kumar et al. [58], and Bernath et al. [55]; the $C^2\Sigma^+ - X^2\Pi$ transitions by Bembenek et al. [59], Ubachs et al. [60], and Heimer [61] for the 0–0 transition, Li et al. [62] for the 1–1 transition, and Herzberg and Johns [63] for the 2–2 transition. Second-order Dunham constants were derived from the spectroscopic constants produced by PGOPHER, and then the Rydberg–Klein–Rees (RKR) method, as implemented in code RKR1 [64], was used to calculate the PECs. These PECs were used in LEVEL to generate the transition moment matrix elements of $R(0)$, which were then used as input to PGOPHER. In a third step, a CH line list was generated using PGOPHER. Finally, this line lists were converted to ExoMol format by Villanueva et al. [22], and partition functions were calculated using the coefficients by Sauval and Tatum [23]. An important part of the conversion to the ExoMol format is to generate a unique set of energies. It is common for experimental line lists in the HITRAN format to have inconsistent energies representing different transitions, including the empirical line list by Masseron et al. [29]. To provide a unique set of energy levels, such instances were replaced by the corresponding mean values. The quantum numbers used are J , v , e/f (rotationless parity), N (rotational quantum number), and the electronic state labels $X^2\Pi$, $A^2\Delta$, $B^2\Sigma^-$ and $C^2\Sigma^+$. Illustrated spectra generated using the line list are given in Figure 2.

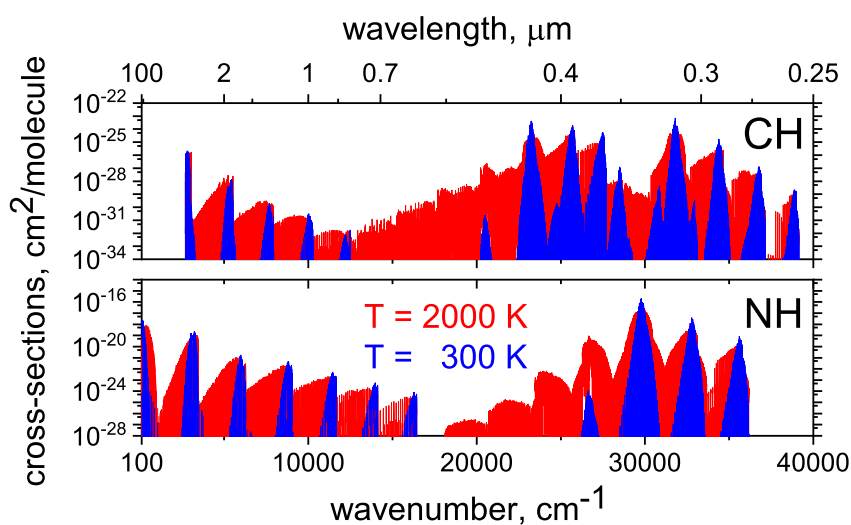


Figure 2. Cross sections of CN and NH computed using line lists by [29–32].

2.3. NH

The NH empirical line list consists of two parts taken from the work of Brooke et al. [30,31], and Fernando et al. [32]. The $X^3\Sigma^-$ ground state line list by Brooke et al. [30] contains ro-vibrational and rotational transitions, including fine structure, for the vibrational bands up to $v' = 6$ with J_{\max} ranging from 25 to 45 for different vibrational bands and is based on the Einstein A and f -values computed using an ab initio DMF which was generated with the internally contracted multi-reference configuration interaction (ic-MRCI) method and an aug-cc-pV6Z basis set. Programs RKR1, LEVEL, and PGOPHER were used to calculate line positions and intensities. Brooke et al. [31] used an improved method to convert the transition matrix elements from Hund's case (b) to produce more

accurate NH transition strengths. A new line list for the $A^3\Pi - X^3\Sigma^-$ electronic band of NH was provided by Fernando et al. [32]. The spectroscopic constants for $A^3\Pi$ and $X^3\Sigma^-$ states were obtained from Ram and Bernath [65] based on Brazier et al. [66] for the $A-X$ transition and Ram et al. [67] for the infrared vibration-rotation and pure rotation lines. High level ab initio calculations were performed with MOLPRO [68] to obtain the $A-X$ transition DMF. PECs and line strengths were calculated with Le Roy's RKR1 and LEVEL programs, respectively. Line intensities and Einstein A values were computed with PGOPHER after converting the Hund's case (b) output of LEVEL to the Hund's case (a) input needed for PGOPHER. Finally, the line lists were compiled into the ExoMol format by Villanueva et al. [22] and the partition functions were calculated following Sauval and Tatum [23]. See Table 4 for the statistical weights used to convert their partition function to the physicists convention used by ExoMol. Quantum numbers used are J, v , electronic state, $F, e/f$ and N . The line list is illustrated in Figure 2.

Table 4. Statistical weights used to convert the partition functions by Sauval and Tatum [23] to ExoMol.

Molecule	g_{ns}	Molecule	g_{ns}
$^{27}\text{Al}^{35}\text{Cl}$	24	$^{24}\text{Mg}^{19}\text{F}$	2
$^{27}\text{Al}^{37}\text{Cl}$	24	$^{25}\text{Mg}^{19}\text{F}$	12
$^{27}\text{Al}^{19}\text{F}$	12	$^{26}\text{Mg}^{19}\text{F}$	2
$^{40}\text{Ca}^{19}\text{F}$	2	$^{23}\text{Na}^{19}\text{F}$	8
$^{42}\text{Ca}^{19}\text{F}$	2	$^{14}\text{N}^1\text{H}$	6
$^{43}\text{Ca}^{19}\text{F}$	16	$^{16}\text{O}^1\text{H}$	2
$^{44}\text{Ca}^{19}\text{F}$	2	$^{16}\text{O}^1\text{H}^+$	2
$^{46}\text{Ca}^{19}\text{F}$	2	$^{12}\text{C}^1\text{H}$	2
$^8\text{Ca}^{19}\text{F}$	2	$^{24}\text{Mg}^1\text{H}$	2
$^{39}\text{K}^{19}\text{F}$	8	$^{48}\text{Ti}^1\text{H}$	2
$^{41}\text{K}^{19}\text{F}$	8	$^{52}\text{Cr}^1\text{H}$	2
$^6\text{Li}^{35}\text{Cl}$	12	$^{56}\text{Fe}^1\text{H}$	2
$^6\text{Li}^{37}\text{Cl}$	12	$^{12}\text{C}_2$	1
$^7\text{Li}^{35}\text{Cl}$	16	$^{12}\text{C}^{31}\text{P}$	2
$^7\text{Li}^{37}\text{Cl}$	16	$^{12}\text{C}^{14}\text{N}$	3
$^6\text{Li}^{19}\text{F}$	6	$^{40}\text{Ca}^1\text{H}$	2
$^7\text{Li}^{19}\text{F}$	8	$^{14}\text{N}_2$	3 & 6

2.4. OH

The OH line list was constructed from two empirical line lists. A line list for the ground electronic state $X^2\Pi$ of OH was produced by Brooke et al. [33] for the vibrational (Meinel system) and pure rotational transitions covering v up to 13 with J_{max} ranging from 9.5 and 59.5, depending on the band. A fit to the molecular constants was performed. This fit was based mainly on that of Bernath and Colin [69] but included some new rotational data from Martin-Drumel et al. [70]. The absolute transition strengths were based on a new DMF, produced from a combination of two high level ab initio methods. A line list for the $A^2\Sigma^+ - X^2\Pi$ electronic band system of OH was calculated by Yousefi et al. [34]. Line positions were taken from Stark et al. [71], Coxon [72], Coxon et al. [73], Derro et al. [74], Yarkony [75] and refitted with PGOPHER. Line intensities were calculated using a new ab initio transition dipole moment function (TDMF) obtained with Molpro 2012. This new TDMF and PECs generated with program RKR1 were used as input to LEVEL which computed matrix elements of the transition dipole moment. The quantum numbers are $J, v, F_1/F_2$ (spin component), and the e/f parity. The line list is illustrated in Figure 3.

Both HITRAN [76] and HITEMP [77] provide line lists for OH; the line lists only cover the ground electronic state $X-X$ transitions and do not use the work of Brooke et al. [33], as also illustrated in Figure 3. In particular, HITEMP was based on the older experimental data by Goldman et al. [78]. The MoLLIST line list is both more accurate and more complete.

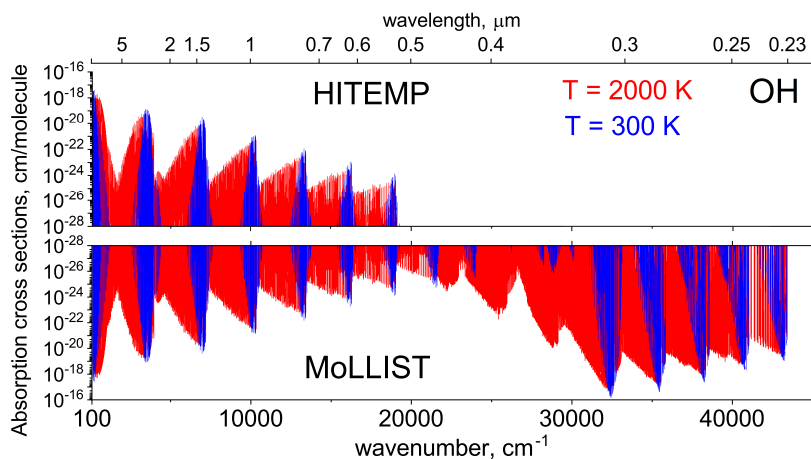


Figure 3. Comparison of the HITEMP [77] and MoLLIST line lists for OH: $T = 300$ and 2000 K absorption cross sections computed using a Doppler line profile. The MoLLIST spectrum is based on the data from Brooke et al. [33].

2.5. OH^+

An OH^+ line list for the $A^3\Pi - X^3\Sigma^-$ band system was produced by Hodges and Bernath [35], Hodges et al. [36]. Hodges and Bernath [35] fitted ground state rotational [79,80] and rovibrational [81,82] data sets using SPCAT/SPFIT [83] with Dunham constants from the Cologne Database for Molecular Spectroscopy (CDMS; Endres et al. [84]). The ground state data were combined with the near-UV and predissociation data [85] and fitted using PGOPHER. Hodges et al. [36] used their analysis of a laboratory spectrum [35] with ab initio methods to calculate infrared and ultraviolet oscillator strengths. These new oscillator strengths include branch dependent intensity corrections, arising from the Herman–Wallis effect. The quantum numbers used are J , v , Electronic state, F and e/f . The line list is illustrated in Figure 4.

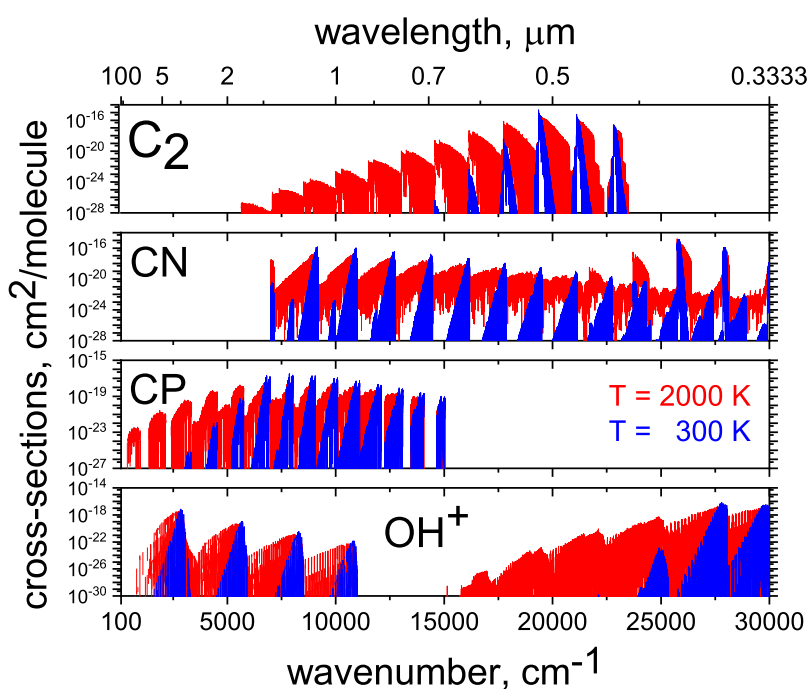


Figure 4. Absorption cross sections of C_2 [45], CN [47], CP [46] and OH^+ [35,36].

2.6. CaF

A line list for the ground state of CaF due Hou and Bernath [37] was based on RCCSD(T) (restricted coupled clusters singles, doubles and approximate triples) ab initio calculations. The RCCSD(T) potential function was represented using the extended Morse oscillator (EMO) potential function and then refined by fitting to the observed lines positions of CaF from Charron et al. [86]. With the EMO potential and the RCCSD(T) dipole moment function, line lists for six isotopes of CaF were computed for $v \leq 10$, $J \leq 123$, $\Delta v = 0 - 10$. Finally, the line lists were compiled into the ExoMol format. Spectra of CaF are illustrated in Figure 5. The quantum numbers used are J and v .

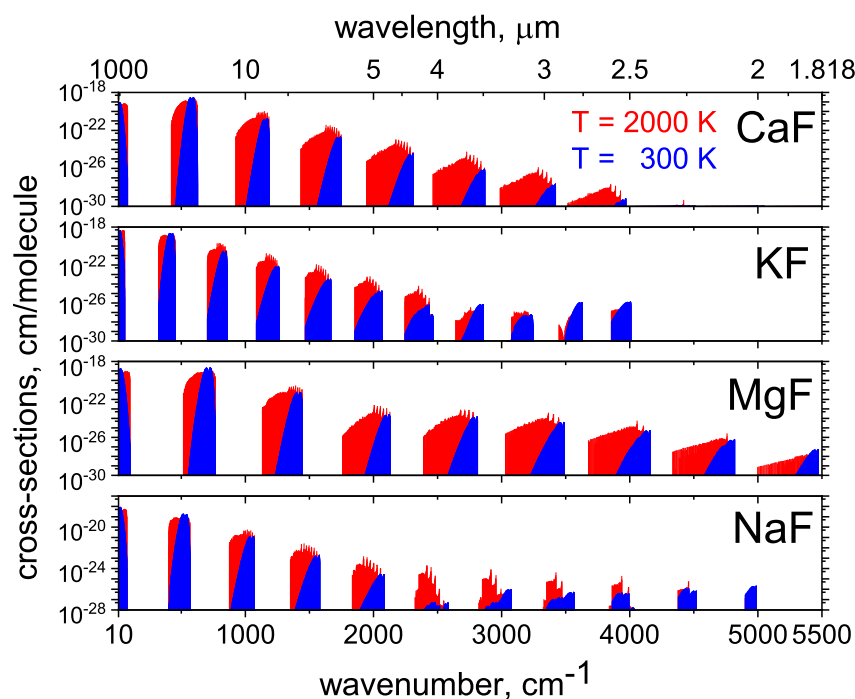


Figure 5. Absorption cross sections of CaF [37], KF and NaF [38], MgF [39].

2.7. KF and NaF

Rotation–vibration line lists for NaF and KF in their ground electronic states were produced by Frohman et al. [38]. Experimental data used were previously measured for infrared transitions up to $v = 8$ and $v = 9$ for KF and NaF by Liu et al. [87] and Muntianu et al. [88]. Additionally, for NaF, three microwave [89] and ten mm-wave [90] lines were used to construct the global line list used for fitting. Six ^{39}KF microwave lines [91,92] and fourteen mm-wave lines [90] were used to construct the global line lists. DMFs were generated from ab initio calculations using the SA-CASSCF (state-averaged complete active space self-consistent field) and ACPF (averaged coupled-pairs functional) methods. PECs were determined by fitting various models to experimental data using the program RKR1 and then LEVEL to generated ro-vibrational levels. PGOPHER was used to calculate Einstein A values and line positions. The quantum numbers used are J and v . The spectra of NaF and KF are illustrated in Figure 5.

2.8. MgF

Line lists for MgF in its $X^2\Sigma^+$ ground states were generated by Hou and Bernath [39]. An EMO PEC was obtained by fitting to observed laboratory vibration–rotation and pure rotational transitions from Barber et al. [93]. Line lists were computed for $v \leq 8$, J , $\Delta v = 0 - 8$ using the EMO PEC and an

analytic DMF in the form of a Padé approximant fitted to ab initio dipole moment data. Finally, the line lists were compiled into ExoMol format (states and trans file), and partition functions were calculated according to Sauval and Tatum [23]. The quantum numbers used include J and v . The spectrum of MgF is illustrated in Figure 5.

2.9. LiCl and LiF

Ro-vibrational line lists for LiF and LiCl in their ground $X^1\Sigma^+$ electronic states were computed by Bittner and Bernath [40]. The ro-vibrational energy levels were calculated using empirical EMO PECs which were determined by direct potential-fitting to the new data from Bittner and Bernath [40] using dPotFit [94]. Ab initio DMCs were obtained using Molpro 2012 with the MRCI/aug-cc-pwCV5Z level of theory and used for the line strength calculations. Program LEVEL was employed to calculate the final line lists. The partition functions of LiF and LiCl were taken from Bittner and Bernath [40] and multiplied by the corresponding statistical nuclear weights, according to the physicists convention. The quantum numbers used are J and v . Spectra computed using these line lists are illustrated in Figure 6.

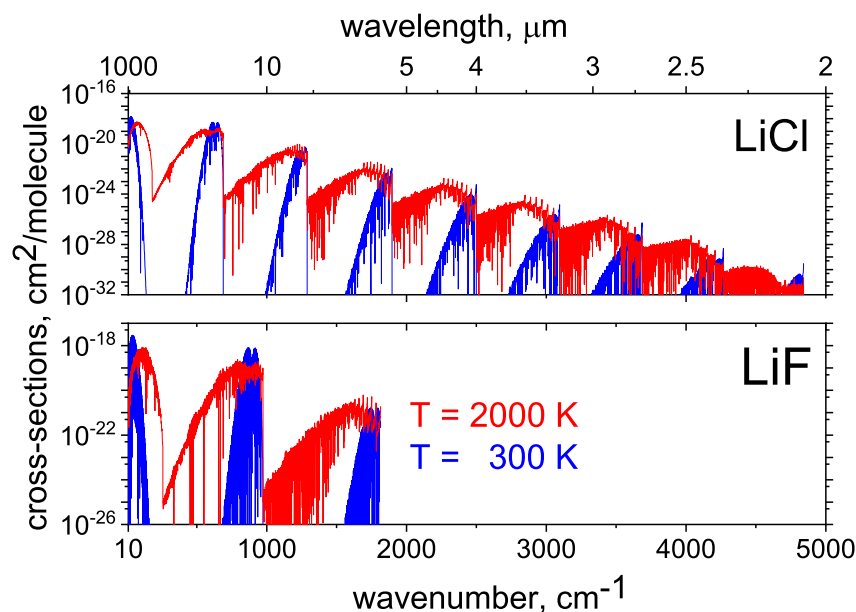


Figure 6. Absorption cross sections of LiCl and LiF from Bittner and Bernath [40].

2.10. MgH

Ro-vibrationally resolved transitions for the $A^2\Pi \rightarrow X^2\Sigma^+$ and $B'^2\Sigma^+ \rightarrow X^2\Sigma^+$ band systems of ^{24}MgH were calculated by GharibNezhad et al. [41]. Empirically-determined analytic PECs [95] for the $X^2\Sigma^+$ state and RKR potentials for the $A^2\Pi$ and $B'^2\Sigma^+$ states were combined with the most recent ab initio TDMCs computed by Mostafanejad and Shayesteh [96] to produce a rovibronic line list. The program LEVEL was used to calculate transition dipole moment and PGOPHER was used to generate the line list. The calculated rovibronic transition frequencies were improved by substituting the term values of the $X^2\Sigma^+$, $A^2\Pi$ and $B'^2\Sigma^+$ states of ^{24}MgH with the empirical values from Shayesteh et al. [97]. Using the ab initio TDMCs, transition frequencies and Hönl–London factors, the Einstein A coefficients were calculated individually for $\sim 30,000$ rovibronic lines of the $A^2\Pi \rightarrow X^2\Sigma^+$ and $B'^2\Sigma^+ \rightarrow X^2\Sigma^+$ systems of ^{24}MgH . The quantum numbers used are J , electronic state, v , N (total angular momentum quantum number excluding spin), F_1/F_2 , and e/f . The spectra computed using these line lists are illustrated in Figure 7.

Note that there are existing ExoMol line lists for isotopologues of MgH which cover rotation–vibration transitions within the ground electronic state [98].

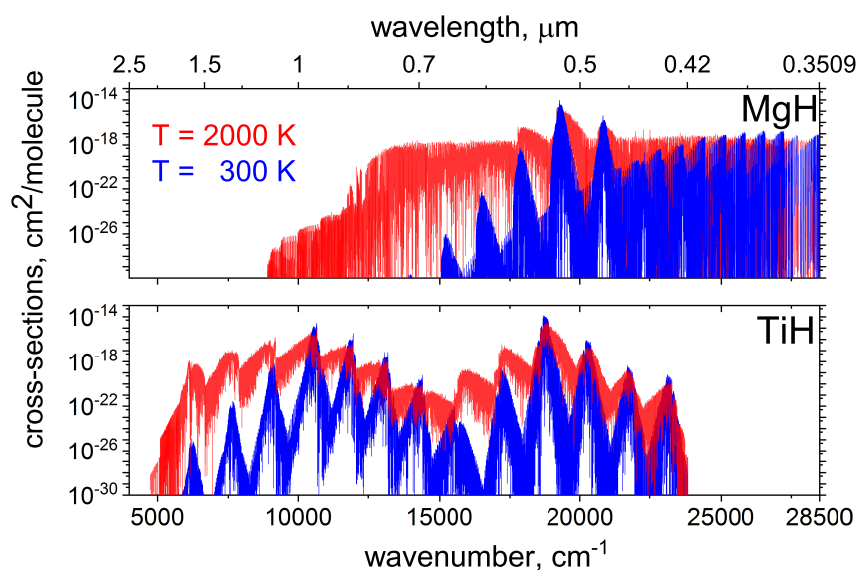


Figure 7. Absorption cross sections of MgH and TiH from GharibNezhad et al. [41] and Burrows et al. [42].

2.11. TiH

A line list for the TiH $B^4\Gamma - X^4\Phi$ and $A^4\Phi - X^4\Phi$ systems were produced by Burrows et al. [42] using a combination of the experimental line positions [99–102] and ab initio transition probabilities. The latter were obtained based on Molpro 2002 calculations using the IC-MRCI/SA-CASSCF level of theory; scalar relativistic effects were accounted for using the Douglas–Kroll–Hess (DKH) approach. The quantum numbers used are J , v , Ω , $+/-$ parity, electronic state. Illustrative spectra of TiH computed using this line list are given in Figure 7.

2.12. CrH

A limited line list for CrH was provided by Chowdhury et al. [43], see Figure 8. The (1,0) band of the $A^6\Sigma^+ - X^6\Sigma^+$ system was observed and rotational assignments for levels with $N \leq 3$ made. These assignments were based on Fourier transform emission spectra [103] for which higher- N lines were assigned. The low- N rotational levels are extensively perturbed, presumably by levels of the $a^4\Sigma^+$, $v = 1$ and $B^6\Pi$, $v = 0$ states. The quantum numbers used are J , v , N , e/f parity, electronic state.

2.13. FeH

A $F^4\Delta - X^4\Delta$ line list ($v = 0, 1, \dots, 4$, $J \leq 50.5$) for FeH was constructed by Dulick et al. [104] based on the experimental energy term values from Phillips et al. [105] ($v = 0, 1, 2$) and an ab initio (IC-MRCI+Q) DTMF. The rovibronic energies were obtained using empirical spectroscopic constants T_v , B_v , A_v and λ_v . The $F-X$ Einstein coefficients were computed using Hönl–London factors and vibrational line strengths based on RKR potentials. The line list contains 25 vibronic bands $v', v'' = 0, 1, 2, 3, 4$ in the $F^4\Delta - X^4\Delta$ system of FeH. The quantum numbers used are J , v , Ω , e/f and electronic states labels ('X4Delta' and 'F4Delta'). The FeH spectra simulated using the line list by Dulick et al. [104] is illustrated in Figure 8.

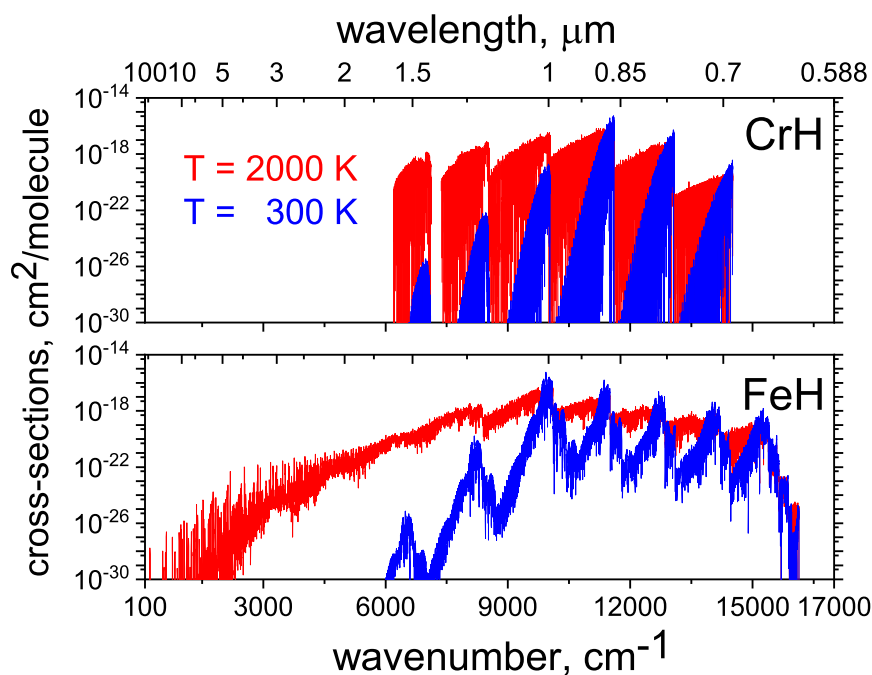


Figure 8. Absorption cross sections of CrH from Chowdhury et al. [43] and FeH from Dulick et al. [104].

2.14. C₂

Brooke et al. [45] calculated rotational line strengths for the C₂ Swan system ($d^3\Pi_g - a^3\Pi_u$) for bands with $v' = 0 - 10$ and $v'' = 0 - 9$ with J_{\max} ranging from 34 to 96, depending on the band using previous observations in 33 vibrational bands [106–110]. Line strengths were based on an ab initio calculation of DTMC using MRCI/aug-cc-pV6Z, taking into account core and core-valence (CV) correlation corrections computed using the aug-cc-pCVQZ basis set and the scalar relativistic energy corrections evaluated via the DKH approach in conjunction with the appropriate cc-pVQZ basis sets. Transition moments were computed by using a bi-orthogonal transformation of the mutually non-orthogonal orbitals of the two states. The quantum chemical calculations were performed using Molpro 2006. The potential energy curves were calculated using the computer program RKR1. PGOPHER was used to calculate Einstein A values and line positions. Rotationless TDMs were calculated using the computer program LEVEL. The quantum numbers used are J , F , e/f , v , and electronic state. This line lists were converted to ExoMol format by Villanueva et al. [22]. The C₂ spectra of Brooke et al. [45] simulated using this line list is illustrated in Figure 4.

The ExoMol database already contains a line list for C₂: Yurchenko et al. [111] constructed a line list, called 8states, because it consists of transitions between the lowest eight electronic states, as part of the ExoMol project. It was produced using a combination of an empirical spectroscopic model and high level ab initio TDMCs. Nuclear motion calculations were performed with the program DUO [11] which allows for full treatment of spin-orbit and other couplings. The 8states line list was improved by replacing the theoretical energies with experimentally determined MARVEL energy values of C₂ [112] and is thus partly based on the same experimental data as the Swan line list of Brooke et al. [45]. 8states is more complete than that of Brooke et al. [45] in that it considers all transitions with $J \leq 190$ for not only the Swan system, but also seven other band systems. For most purposes, 8states provides a more appropriate starting point and the MoLLIST of Brooke et al. [45] is included in case it is needed for specialist applications.

2.15. CP

Ram et al. [46] calculated line strengths for transitions in the $A^2\Pi - X^2\Sigma^+$ band system of CP, which include the effect of rotation on the vibrational wavefunctions (the Herman–Wallis effect), using the programs PGOPHER and LEVEL, based on experimental data due to Ram and Bernath [113], Ram et al. [114], Saito et al. [115], Klein et al. [116]. RKR PECs for the $A^2\Pi$ and $X^2\Sigma^+$ states were constructed using spectroscopic constants from high resolution spectra. The RKR potentials of the two states, and ab initio electronic TDMFs of this from [117] were used in LEVEL to produce transition dipole moment matrix elements. The matrix elements were then converted from Hund's case (b) to (a), and used in PGOPHER to generate a line list containing observed and calculated wavenumbers, Einstein A coefficients and f -values for 75 bands with $v = 0-8$ for both states. Quantum numbers used are J , electronic state, v , F and e/f . Spectra of CP of simulated using this line list are illustrated in Figure 4.

2.16. CN

The line list is due to Brooke et al. [47]. RKR PECs for the $A^2\Pi$, $B^2\Sigma^+$, and $X^2\Sigma^+$ states were computed using spectroscopic constants from the $A^2\Pi - X^2\Sigma^+$ and $B^2\Sigma^+ - X^2\Sigma^+$ transitions based on the experimental data from Brooke et al. [47], Ram et al. [118,119], Davis et al. [120], Horaka et al. [121]. New electronic TDMFs for these systems and a dipole moment function for the $X^2\Sigma^+$ state were generated from high level ab initio calculations and used in LEVEL to produce transition dipole moment matrix elements for a large number of vibrational bands. PGOPHER was then used to calculate Einstein A coefficients, and a line list was generated containing the observed and calculated wavenumbers, Einstein A coefficients and f -values for 290 bands of the $A^2\Pi - X^2\Sigma^+$ system with $v' = 0-22$, $v'' = 0-15$, 250 bands of the $B^2\Sigma^+ - X^2\Sigma^+$ system with $v' = 0-15$, $v'' = 0-15$ and 120 bands of the ro-vibrational transitions within the $X^2\Sigma^+$ state with $v = 0-15$. The quantum numbers used are J , electronic state, v , F and e/f . The CM spectra of Brooke et al. [47] simulated using this line list is illustrated in Figure 4.

2.17. CaH

The CaH line list ($X-X$, $A-X$, $B-X$, $E-X$) is based on the experiment of Shayesteh et al. [49], Ram et al. [122]; see Figure 9. Einstein A coefficients and absolute line intensities of $E^2\Pi - X^2\Sigma^+$ transitions of CaH were calculated by Li et al. [48]. Potential energy functions for both $E^2\Pi$ and $X^2\Sigma^+$ states of CaH were constructed using the purely numerical RKR method with the Kaiser correction and the effective Dunham coefficients from Ram et al. [122]. These RKR potential curves and a high-level ab initio TDMF from Weck et al. [123] were then employed in LEVEL to calculate a transition dipole moment matrix elements for the 10 bands involving $v' = 0, 1$ of the $E^2\Pi$ state and $v'' = 0, 1, 2, 3, 4$ of the $X^2\Sigma^+$ state using the rotational line strength factors (Hönl–London factors) derived for the intermediate coupling case between Hund's case (a) and (b). The computed transition dipole moments and the spectroscopic constants from Ram et al. [122] were combined to generate line lists containing Einstein A coefficients and absolute line intensities for the $X^2\Sigma^+ - X^2\Sigma^+$ and $E^2\Pi - X^2\Sigma^+$ systems of CaH for J -values up to 50.5. We used the line positions from Shayesteh et al. [49], Ram et al. [122] to reconstruct the energy levels using the MARVEL procedure [124]. The Einstein coefficients of the $A^2\Pi - X^2\Sigma^+$, $B^2\Sigma^+ - X^2\Sigma^+$ system were taken from Alavi and Shayesteh [125]. The quantum numbers used are J , e/f , v and electronic state.

Note that there is an existing ExoMol line list for ^{40}CaH which covers rotation–vibration transitions within the ground electronic state [98].

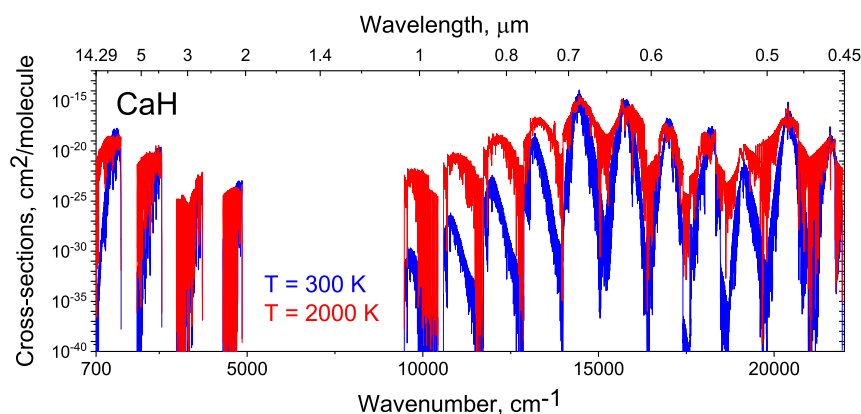


Figure 9. Absorption cross sections of CaH from Li et al. [48], Shayesteh et al. [49], Alavi and Shayesteh [125].

2.18. N_2

The new line list for triplet states of N_2 was produced by Western et al. [21] using experimental data from Boesch and Reiners [126], see Figure 10; the line list includes the $B^3\Pi_g-A^3\Sigma_u^+$, $B'^3\Sigma_u^- - B^3\Pi_g$, $W^3\Delta_u - B^3\Pi_g$ systems. Their analysis used high-level ab initio calculations of PECs, TDMFs, and spin-orbit coupling constants to prepare the model and extend the potential range of applicability. Final line list calculations were performed with PGOPHER. The partition function is based on energies of the singlet ($X^1\Sigma_g^+$) ground electronic state of N_2 computed using the temperature points of Barklem and Collet [24] interpolated on a 1 K grid from 0 to 10,000 K using cubic splines. The ExoMol name of the line list is WCCRMT.

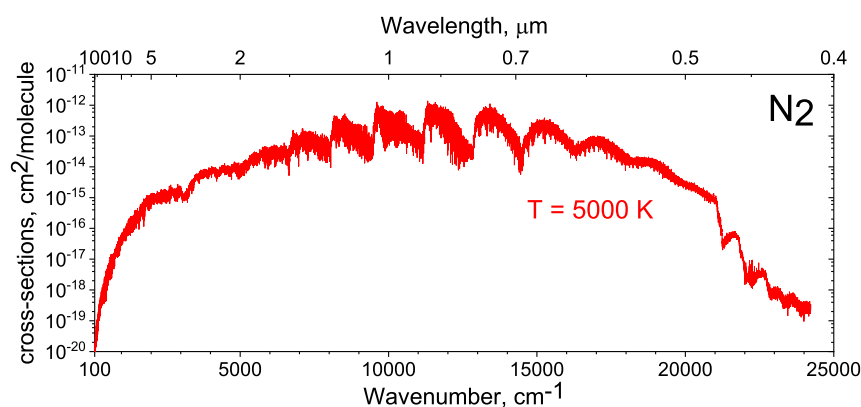


Figure 10. Line lists for N_2 from Western et al. [21].

2.19. Lifetimes

Lifetimes for each state were generated with ExoCross [52] using the methodology of Tennyson et al. [27]. Examples of lifetimes computed using the empirical line lists from Bernath's group are shown in Figure 11.

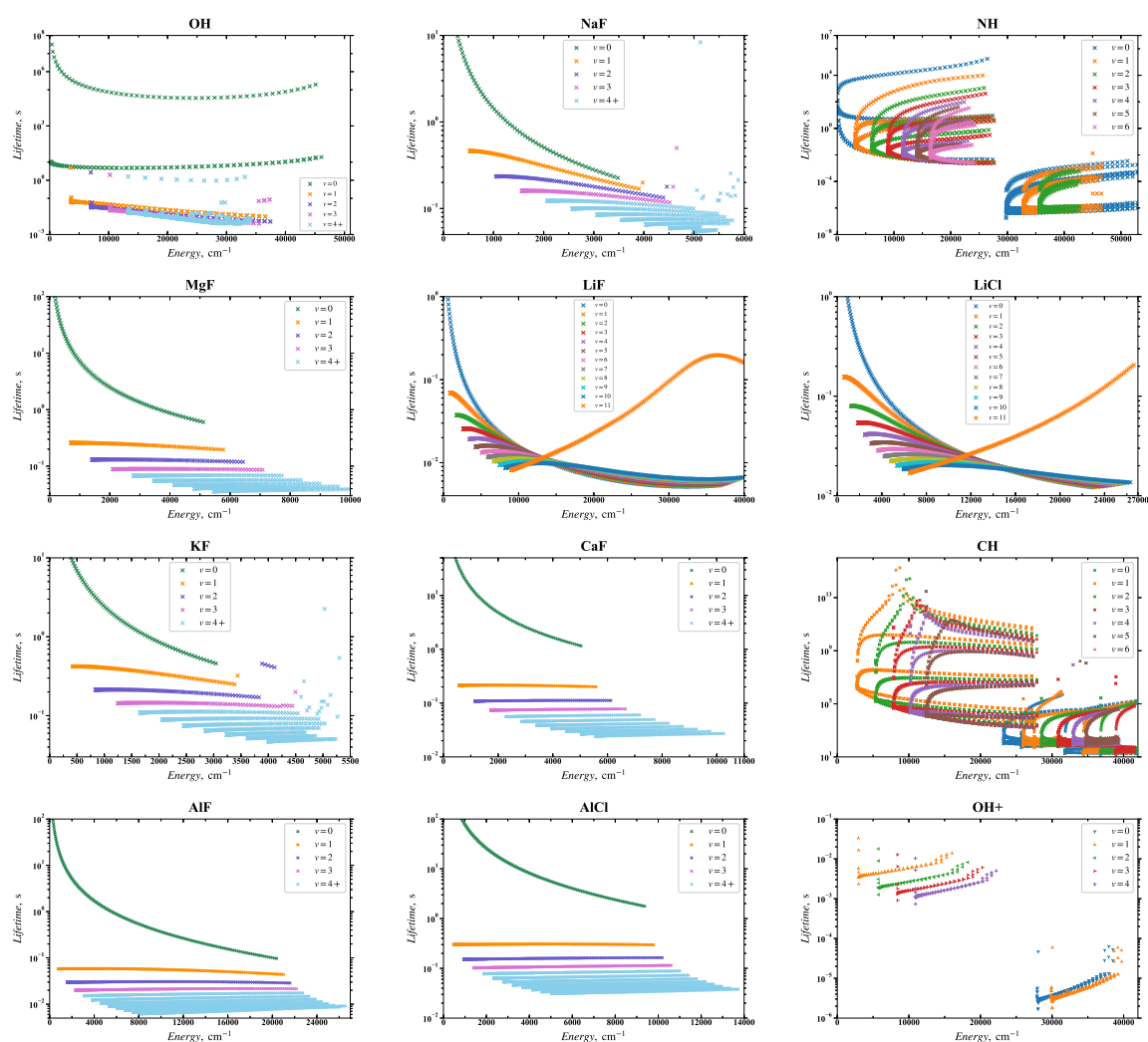


Figure 11. Lifetimes as a function of state energy for the line lists considered in this article. The plots give results for the main isotopologue only.

3. Conclusions

The ExoMol database provides molecular line lists valid over extended temperature ranges for many molecules. This paper describes the inclusion in the database of a new set of experimentally generated line lists which were produced externally to the main ExoMol activity. Most of these line lists (all except the one for N_2) are from the MoLLIST data set <http://bernath.uwaterloo.ca/molecularlists.php> [18]. Inclusion of these line lists significantly improves the coverage of the ExoMol database. They will form an important part of the upcoming release of the database [20].

Author Contributions: Y.W. constructed the new line lists in discussion with S.N.Y. All authors contributed to writing the manuscript. All authors have read and agreed to the published version of the manuscript.

Funding: This work was supported by the UK Science and Technology Research Council (STFC) No. ST/R000476/1. Yixin Wang's visit was supported by Physics Boling Class in Nankai University.

Acknowledgments: Yueqi "Zoe" Na's help with the ExoMol database is greatly appreciated. We thank Peter F. Bernath for many helpful discussions and for encouraging us to use MoLLIST data; we thank Colin Western for help with the N_2 line list and Geronimo L. Villanueva for helping with line lists for CH, NH, and C_2 .

Conflicts of Interest: The authors declare no conflict of interest.

References

1. Tennyson, J.; Yurchenko, S.N. ExoMol: Molecular line lists for exoplanet and other atmospheres. *Mon. Not. R. Astron. Soc.* **2012**, *425*, 21–33. [[CrossRef](#)]
2. Lodi, L.; Tennyson, J. Theoretical methods for small-molecule ro-vibrational spectroscopy. *J. Phys. B At. Mol. Opt. Phys.* **2010**, *43*, 133001. [[CrossRef](#)]
3. Tennyson, J.; Yurchenko, S.N. The ExoMol project: Software for computing molecular line lists. *Intern. J. Quantum Chem.* **2017**, *117*, 92–103. [[CrossRef](#)]
4. McKemmish, L.K.; Yurchenko, S.N.; Tennyson, J. Ab initio calculations to support accurate modelling of the rovibronic spectroscopy calculations of vanadium monoxide (VO). *Mol. Phys.* **2016**, *114*, 3232–3248. [[CrossRef](#)]
5. Tennyson, J. Accurate variational calculations for line lists to model the vibration rotation spectra of hot astrophysical atmospheres. *WIREs Comput. Mol. Sci.* **2012**, *2*, 698–715. [[CrossRef](#)]
6. Tennyson, J.; Yurchenko, S.N. Laboratory spectra of hot molecules: Data needs for hot super-Earth exoplanets. *Mol. Astrophys.* **2017**, *8*, 1–18. [[CrossRef](#)]
7. Tennyson, J. Vibration-rotation transition dipoles from first principles. *J. Mol. Spectrosc.* **2014**, *298*, 1–6. [[CrossRef](#)]
8. Zak, E.J.; Tennyson, J.; Polyansky, O.L.; Lodi, L.; Tashkun, S.A.; Perevalov, V.I. A room temperature CO₂ line list with Ab Initio Comput. Intensities. *J. Quant. Spectrosc. Radiat. Transf.* **2016**, *177*, 31–42. [[CrossRef](#)]
9. Yurchenko, S.N.; Barber, R.J.; Tennyson, J.; Thiel, W.; Jensen, P. Towards efficient refinement of molecular potential energy surfaces: Ammonia as a case study. *J. Mol. Spectrosc.* **2011**, *268*, 123–129. [[CrossRef](#)]
10. Tennyson, J.; Lodi, L.; McKemmish, L.K.; Yurchenko, S.N. The ab initio calculation of spectra of open shell diatomic molecules. *J. Phys. B At. Mol. Opt. Phys.* **2016**, *49*, 102001. [[CrossRef](#)]
11. Yurchenko, S.N.; Lodi, L.; Tennyson, J.; Stolyarov, A.V. Duo: A general program for calculating spectra of diatomic molecules. *Comput. Phys. Commun.* **2016**, *202*, 262–275. [[CrossRef](#)]
12. Barber, R.J.; Strange, J.K.; Hill, C.; Polyansky, O.L.; Mellau, G.C.; Yurchenko, S.N.; Tennyson, J. ExoMol line lists—III. An improved hot rotation-vibration line list for HCN and HNC. *Mon. Not. R. Astron. Soc.* **2014**, *437*, 1828–1835. [[CrossRef](#)]
13. Tennyson, J.; Yurchenko, S.N.; Al-Refaie, A.F.; Barton, E.J.; Chubb, K.L.; Coles, P.A.; Diamantopoulou, S.; Gorman, M.N.; Hill, C.; Lam, A.Z.; et al. The ExoMol database: Molecular line lists for exoplanet and other hot atmospheres. *J. Mol. Spectrosc.* **2016**, *327*, 73–94. [[CrossRef](#)]
14. Bernath, P.F. Molecular astronomy of cool stars and sub-stellar objects. *Int. Rev. Phys. Chem.* **2009**, *28*, 681–709. [[CrossRef](#)]
15. Yurchenko, S.N.; Barber, R.J.; Tennyson, J. A variationally computed hot line list for NH₃. *Mon. Not. R. Astron. Soc.* **2011**, *413*, 1828–1834. [[CrossRef](#)]
16. Western, C.M. PGOPHER: A program for simulating rotational, vibrational and electronic spectra. *J. Quant. Spectrosc. Radiat. Transf.* **2017**, *186*, 221–242. [[CrossRef](#)]
17. Le Roy, R.J. LEVEL: A Computer Program for Solving the Radial Schrödinger Equation for Bound and Quasibound Levels. *J. Quant. Spectrosc. Radiat. Transf.* **2017**, *186*, 167–178. [[CrossRef](#)]
18. Bernath, P.F. MoLLIST: Molecular Line Lists, Intensities and Spectra. *J. Quant. Spectrosc. Radiat. Transf.* **2020**, *240*, 106687. [[CrossRef](#)]
19. Semenov, M.; Yurchenko, S.N.; Tennyson, J. Predicted Landé g-factors for open shell diatomic molecules. *J. Mol. Spectrosc.* **2017**, *330*, 57–62. [[CrossRef](#)]
20. Tennyson, J.; Yurchenko, S.N. The 2020 release of the ExoMol database: Molecular line lists for exoplanet and other hot atmospheres. *J. Quant. Spectrosc. Radiat. Transf.* **2020**, in preparation.
21. Western, C.M.; Carter-Blatchford, L.; Crozet, P.; Ross, A.J.; Morville, J.; Tokaryk, D.W. The spectrum of N₂ from 4,500 to 15,700 cm⁻¹ revisited with PGOPHER. *J. Quant. Spectrosc. Radiat. Transf.* **2018**, *219*, 127–141. [[CrossRef](#)]
22. Villanueva, G.L.; Smith, M.D.; Protopapa, S.; Faggi, S.; Mandell, A.M. Planetary Spectrum Generator: An accurate online radiative transfer suite for atmospheres, comets, small bodies and exoplanets. *J. Quant. Spectrosc. Radiat. Transf.* **2018**, *217*, 86–104. [[CrossRef](#)]
23. Sauval, A.J.; Tatum, J.B. A set of partition functions and equilibrium constants for 300 diatomic molecules of astrophysical interest. *Astrophys. J. Suppl.* **1984**, *56*, 193–209. [[CrossRef](#)]

24. Barklem, P.S.; Collet, R. Partition functions and equilibrium constants for diatomic molecules and atoms of astrophysical interest. *Astron. Astrophys.* **2016**, *588*, A96. [[CrossRef](#)]
25. Pavlenko, Y.V.; Yurchenko, S.N.; Tennyson, J. Analysis of first overtone bands of isotopologues of CO and SiO in stellar spectr. *Astron. Astrophys.* **2020**, *633*, A52. [[CrossRef](#)]
26. Gamache, R.R.; Roller, C.; Lopes, E.; Gordon, I.E.; Rothman, L.S.; Polyansky, O.L.; Zobov, N.F.; Kyuberis, A.A.; Tennyson, J.; Yurchenko, S.N.; et al. Total Internal Partition Sums for 167 isotopologues of 53 molecules important in planetary atmospheres: Application to HITRAN2016 and beyond. *J. Quant. Spectrosc. Radiat. Transf.* **2017**, *203*, 70–87. [[CrossRef](#)]
27. Tennyson, J.; Hulme, K.; Naim, O.K.; Yurchenko, S.N. Radiative lifetimes and cooling functions for astrophysically important molecules. *J. Phys. B At. Mol. Opt. Phys.* **2016**, *49*, 044002. [[CrossRef](#)]
28. Yousefi, M.; Bernath, P.F. Line Lists for AlF and AlCl in the $X^1\Sigma^+$ Ground State. *Astrophys. J. Suppl.* **2018**, *237*, 8. [[CrossRef](#)]
29. Masseron, T.; Plez, B.; Van Eck, S.; Colin, R.; Daoutidis, I.; Godefroid, M.; Coheur, P.F.; Bernath, P.; Jorissen, A.; Christlieb, N. CH in stellar atmospheres: An extensive linelist. *Astron. Astrophys.* **2014**, *571*, A47. [[CrossRef](#)]
30. Brooke, J.S.A.; Bernath, P.F.; Western, C.M.; van Hemert, M.C.; Groenenboom, G.C. Line strengths of rovibrational and rotational transitions within the $X^3\Sigma^-$ ground state of NH. *J. Chem. Phys.* **2014**, *141*, 054310. [[CrossRef](#)]
31. Brooke, J.S.A.; Bernath, P.F.; Western, C.M. Note: Improved line strengths of rovibrational and rotational transitions within the $X^3\Sigma^-$ ground state of NH. *J. Chem. Phys.* **2015**, *143*, 026101. [[CrossRef](#)] [[PubMed](#)]
32. Fernando, A.M.; Bernath, P.F.; Hodges, J.N.; Masseron, T. A new linelist for the $A^3\Pi - X^3\Sigma^-$ transition of the NH free radical. *J. Quant. Spectrosc. Radiat. Transf.* **2018**, *217*, 29–34. [[CrossRef](#)]
33. Brooke, J.S.A.; Bernath, P.F.; Western, C.M.; Sneden, C.; AfÅyar, M.; Li, G.; Gordon, I.E. Line strengths of rovibrational and rotational transitions in the $X^2\Pi$ ground state of OH. *J. Quant. Spectrosc. Radiat. Transf.* **2016**, *138*, 142–157. [[CrossRef](#)]
34. Yousefi, M.; Bernath, P.F.; Hodges, J.; Masseron, T. A new line list for the $A^2\Sigma^+ - X^2\Pi$ electronic transition of OH. *J. Quant. Spectrosc. Radiat. Transf.* **2018**, *217*, 416–424. [[CrossRef](#)]
35. Hodges, J.N.; Bernath, P.F. Fourier Transform Spectroscopy of the $A^3\Pi - X^3\Sigma^-$ Transition of OH⁺. *Astrophys. J.* **2017**, *840*, 81. [[CrossRef](#)]
36. Hodges, J.N.; Bittner, D.M.; Bernath, P.F. Improved Ultraviolet and Infrared Oscillator Strengths for OH⁺. *Astrophys. J.* **2018**, *855*. [[CrossRef](#)]
37. Hou, S.; Bernath, P.F. Line list for the ground state of CaF. *J. Quant. Spectrosc. Radiat. Transf.* **2018**, *210*, 44–51. [[CrossRef](#)]
38. Frohman, D.J.; Bernath, P.F.; Brooke, J.S.A. Molecular line lists: The ro-vibrational spectra of NaF and KF. *J. Quant. Spectrosc. Radiat. Transf.* **2016**, *169*, 104–110. [[CrossRef](#)]
39. Hou, S.; Bernath, P.F. Line list for the MgF ground state. *J. Quant. Spectrosc. Radiat. Transf.* **2017**, *203*, 511–516. [[CrossRef](#)]
40. Bittner, D.M.; Bernath, P.F. Line Lists for LiF and LiCl in the $X^1\Sigma^+$ Ground State. *Astrophys. J. Suppl.* **2018**, *235*, 8. [[CrossRef](#)]
41. GharibNezhad, E.; Shayesteh, A.; Bernath, P.F. Einstein A coefficients for rovibronic lines of the $A^2\Pi \rightarrow X^2\Sigma^+$ and $B'^2\Sigma^+ \rightarrow X^2\Sigma^+$ transitions of MgH. *Mon. Not. R. Astron. Soc.* **2013**, *432*, 2043–2047. [[CrossRef](#)]
42. Burrows, A.; Dulick, M.; Bauschlicher, C.W.; Bernath, P.F.; Ram, R.S.; Sharp, C.M.; Milsom, J.A. Spectroscopic constants, abundances, and opacities of the TiH molecule. *Astrophys. J.* **2005**, *624*, 988–1002. [[CrossRef](#)]
43. Chowdhury, P.K.; Merer, A.J.; Rixon, S.J.; Bernath, P.F.; Ram, R.S. Low-N lines of the $A^6\Sigma^+ - X^6\Sigma^+$ (1,0) band of CrH. *PCCP* **2006**, *8*, 822–826. [[CrossRef](#)] [[PubMed](#)]
44. Wende, S.; Reiners, A.; Seifahrt, A.; Bernath, P.F. CRILES spectroscopy and empirical line-by-line identification of FeH molecular absorption in an M dwarf. *Astron. Astrophys.* **2010**, *523*, A58. [[CrossRef](#)]
45. Brooke, J.S.A.; Bernath, P.F.; Schmidt, T.W.; Bacskay, G.B. Line strengths and updated molecular constants for the C₂ Swan system. *J. Quant. Spectrosc. Radiat. Transf.* **2013**, *124*, 11–20. [[CrossRef](#)]
46. Ram, R.S.; Brooke, J.S.A.; Western, C.M.; Bernath, P.F. Einstein A-values and oscillator strengths of the $A^2\Pi - X^2\Sigma^+$ system of CP. *J. Quant. Spectrosc. Radiat. Transf.* **2014**, *138*, 107–115. [[CrossRef](#)]
47. Brooke, J.S.A.; Ram, R.S.; Western, C.M.; Li, G.; Schwenke, D.W.; Bernath, P.F. Einstein A coefficients and oscillator strengths for the $A^2\Pi - X^2\Sigma^+$ (red) and $B^2\Sigma^+ - X^2\Sigma^+$ violet systems and rovibrational transitions in the $X^2\Sigma^+$ state of CN. *Astrophys. J. Suppl.* **2014**, *210*, 23. [[CrossRef](#)]

48. Li, G.; Harrison, J.J.; Ram, R.S.; Western, C.M.; Bernath, P.F. Einstein A coefficients and absolute line intensities for the $E^2\Pi - X^2\Sigma^+$ transition of CaH. *J. Quant. Spectrosc. Radiat. Transf.* **2012**, *113*, 67–74. [[CrossRef](#)]
49. Shayesteh, A.; Ram, R.S.; Bernath, P.F. Fourier transform emission spectra of the $A^2\Pi \rightarrow X^2\Sigma^+$ and $B^2\Sigma^+ \rightarrow X^2\Sigma^+$ band systems of CaH. *J. Mol. Spectrosc.* **2013**, *288*, 46–51. [[CrossRef](#)]
50. Zhang, K.; Guo, B.; Braun, V.; Dulick, M.; Bernath, P. Infrared emission spectroscopy of BF and AlF. *J. Mol. Spectrosc.* **1995**, *170*, 82–93. [[CrossRef](#)]
51. Hedderich, H.; Dulick, M.; Bernath, P. High resolution emission spectroscopy of AlCl at 20 μ . *J. Chem. Phys.* **1993**, *99*, 8363–8370. [[CrossRef](#)]
52. Yurchenko, S.N.; Al-Refaie, A.F.; Tennyson, J. ExoCross: A general program for generating spectra from molecular line lists. *Astron. Astrophys.* **2018**, *614*, A131. [[CrossRef](#)]
53. Colin, R.; Bernath, P.F. Revised molecular constants and term values for the $X^2\Pi$ state of CH. *J. Mol. Spectrosc.* **2010**, *263*, 120–122. [[CrossRef](#)]
54. Bernath, P.F.; McElroy, C.T.; Abrams, M.; Boone, C.D.; Butler, M.; Camy-Peyret, C.; Carleer, M.; Clerbaux, C.; Coheur, P.F.; Colin, R.; et al. Atmospheric chemistry experiment (ACE): Mission overview. *Geophys. Res. Lett.* **2005**, *32*. [[CrossRef](#)]
55. Bernath, P.; Brazier, C.; Olsen, T.; Hailey, R.; Fernando, W.; Woods, C.; Hardwick, J. Spectroscopy of the CH free radical. *J. Mol. Spectrosc.* **1991**, *147*, 16–26. [[CrossRef](#)]
56. Zachwieja, M. New Investigations of the $A^2\Delta - X^2\Pi$ Band System in the CH Radical and a New Reduction of the Vibration-Rotation Spectrum of CH from the ATMOS Spectra. *J. Mol. Spectrosc.* **1995**, *170*, 285–309. [[CrossRef](#)]
57. Kepa, R.; Para, A.; Rytel, M.; Zachwieja, M. New Spectroscopic Analysis of the $B^2\Sigma^- - X^2\Pi$ Band System of the CH Molecule. *J. Mol. Spectrosc.* **1996**, *178*, 189–193. [[CrossRef](#)]
58. Kumar, A.; Hsiao, C.C.; Hung, W.C.; Lee, Y.P. Highly predissociative levels of CH $B^2\Sigma^-$ state detected with two-color resonant four-wave mixing spectroscopy. *J. Chem. Phys.* **1998**, *109*, 3824–3830. [[CrossRef](#)]
59. Bembenek, Z.; Ke, R.; Rytel, M. Analysis of the 0–0 Band of the $C^2\Sigma^+ - X^2\Pi$ Band System in the ^{12}CH and ^{13}CH Isotopic Radicals. *J. Mol. Spectrosc.* **1997**, *183*, 1–5. [[CrossRef](#)]
60. Ubachs, W.; Meyer, G.; Ter Meulen, J.; Dymanus, A. Hyperfine structure and lifetime of the $C^2\Sigma^+$, $v = 0$ state of CH. *J. Chem. Phys.* **1986**, *84*, 3032–3041. [[CrossRef](#)]
61. Heimer, T. Untersuchung über die Kohlenwasserstoffbande λ 3143. *Z. Für Phys.* **1932**, *78*, 771–780. [[CrossRef](#)]
62. Li, X.; Kumar, A.; Hsiao, C.C.; Lee, Y.P. Two-Color Resonant Four-Wave Mixing Spectra of the $C^2\Sigma^+ - X^2\Pi$ (1 - 1) Band of CH in a Flame. *J. Phys. Chem. A* **1999**, *103*, 6162–6166. [[CrossRef](#)]
63. Herzberg, G.; Johns, J. New spectra of the CH molecule. *Astrophys. J.* **1969**, *158*, 399–418. [[CrossRef](#)]
64. Le Roy, R.J. RKR1: A computer program implementing the first-order RKR method for determining diatomic molecule potential energy functions. *J. Quant. Spectrosc. Radiat. Transf.* **2017**, *186*, 158–166. [[CrossRef](#)]
65. Ram, R.; Bernath, P. Revised molecular constants and term values for the $X^3\Sigma^-$ and $A^3\Pi$ states of NH. *J. Mol. Spectrosc.* **2010**, *260*, 115–119. [[CrossRef](#)]
66. Brazier, C.; Ram, R.; Bernath, P. Fourier transform spectroscopy of the $A^3\Pi - X^3\Sigma^-$ transition of NH. *J. Mol. Spectrosc.* **1986**, *120*, 381–402. [[CrossRef](#)]
67. Ram, R.; Bernath, P.; Hinkle, K. Infrared emission spectroscopy of NH: Comparison of a cryogenic echelle spectrograph with a Fourier transform spectrometer. *J. Chem. Phys.* **1999**, *110*, 5557–5563. [[CrossRef](#)]
68. Werner, H.J.; Knowles, P.J.; Knizia, G.; Manby, F.R.; Schütz, M. Molpro: A general-purpose quantum chemistry program package. *WIREs Comput. Mol. Sci.* **2012**, *2*, 242–253. [[CrossRef](#)]
69. Bernath, P.F.; Colin, R. Revised molecular constants and term values for the $X^2\Pi$ and $B^2\Sigma^+$ states of OH. *J. Mol. Spectrosc.* **2009**, *257*, 20–23. [[CrossRef](#)]
70. Martin-Drumel, M.; Pirali, O.; Balcon, D.; Brechignac, P.; Roy, P.; Vervloet, M. High resolution far-infrared Fourier transform spectroscopy of radicals at the AILES beamline of SOLEIL synchrotron facility. *Rev. Sci. Instrum.* **2011**, *82*, 113106. [[CrossRef](#)]
71. Stark, G.; Brault, J.W.; Abrams, M.C. Fourier-transform spectra of the $A^2\Sigma^+ - X^2\Pi$ $\Delta v = 0$ bands of OH and OD. *JOSA B* **1994**, *11*, 3–32. [[CrossRef](#)]
72. Coxon, J. Optimum molecular constants and term values for the $X^2\Pi$ ($v \leq 5$) and $A^2\Sigma^+$ ($v \leq 3$) states of OH. *Can. J. Phys.* **1980**, *58*, 933–949. [[CrossRef](#)]

73. Coxon, J.A.; Sappey, A.D.; Copeland, R.A. Molecular constants and term values for the hydroxyl radical, OH: The $X^2\Pi$ ($v = 8, 12$), $A^2\Sigma^+$ ($v = 4-9$), $B^2\Sigma^+$ ($v = 0, 1$), and $C^2\Sigma^+$ ($v = 0, 1$) states. *J. Mol. Spectrosc.* **1991**, *145*, 41–55. [[CrossRef](#)]
74. Derro, E.L.; Pollack, I.B.; Dempsey, L.P.; Greenslade, M.E.; Lei, Y.; Radenović, D.Č.; Lester, M.I. Fluorescence-dip infrared spectroscopy and predissociation dynamics of OH $A^2\Sigma^+$ ($v = 4$) radicals. *J. Chem. Phys.* **2005**, *122*, 244313. [[CrossRef](#)] [[PubMed](#)]
75. Yarkony, D.R. A theoretical treatment of the predissociation of the individual rovibronic levels of OH/OD ($A^2\Sigma^+$). *J. Chem. Phys.* **1992**, *97*, 1838–1849. [[CrossRef](#)]
76. Gordon, I.E.; Rothman, L.S.; Hill, C.; Kochanov, R.V.; Tan, Y.; Bernath, P.F.; Birk, M.; Boudon, V.; Campargue, A.; Chance, K.V.; et al. The HITRAN 2016 molecular spectroscopic database. *J. Quant. Spectrosc. Radiat. Transf.* **2017**, *203*, 3–69. [[CrossRef](#)]
77. Rothman, L.; Gordon, I.; Barber, R.; Dothe, H.; Gamache, R.; Goldman, A.; Perevalov, V.; Tashkun, S.; Tennyson, J. HITEMP, the high-temperature molecular spectroscopic database. *J. Quant. Spectrosc. Radiat. Transf.* **2010**, *111*, 2139–2150. [[CrossRef](#)]
78. Goldman, A.; Schoenfeld, W.G.; Goorvitch, D.; Chackerian, C.; Dothe, H.; Melen, F.; Abrams, M.C.; Selby, J.E.A. Updated line parameters for OH $X^2\Pi - X^2\Pi(v'', v')$ transitions. *J. Quant. Spectrosc. Radiat. Transf.* **1998**, *59*, 453–469. [[CrossRef](#)]
79. Bekooy, J.P.; Verhoeve, P.; Meerts, W.L.; Dymanus, A. Submillimeter spectroscopy on OH⁺: The rotational transition at 1 THz. *JCP* **1985**, *82*, 3868–3869. [[CrossRef](#)]
80. Liu, D.J.; Ho, W.C.; Oka, T. Rotational spectroscopy of molecular ions using diode lasers. *J. Chem. Phys.* **1987**, *87*, 2442–2446. [[CrossRef](#)]
81. Rehfuss, B.D.; Jagod, M.F.; Xu, L.W.; Oka, T. Infrared spectroscopy of highly excited vibrational levels of the hydroxyl ion, OH⁺. *J. Mol. Spectrosc.* **1992**, *151*, 59–70. [[CrossRef](#)]
82. Markus, C.R.; Hodges, J.N.; Perry, A.J.; Kocheril, G.S.; Müller, H.S.; McCall, B.J. High precision rovibrational spectroscopy of OH⁺. *Astrophys. J.* **2016**, *817*, 138. [[CrossRef](#)]
83. Pickett, H.M. The fitting and prediction of vibration-rotation spectra with spin interactions. *J. Mol. Spectrosc.* **1991**, *148*, 371–377. [[CrossRef](#)]
84. Endres, C.P.; Schlemmer, S.; Schilke, P.; Stutzki, J.; Müller, H.S.P. The cologne database for molecular spectroscopy, CDMS, in the virtual atomic and molecular data centre, VAMDC. *J. Mol. Spectrosc.* **2016**, *327*, 95–104. [[CrossRef](#)]
85. Rodgers, D.J.; Batey, A.; Sarre, P.J. High-resolution laser spectroscopy and photodissociation dynamics of OH⁺. *Mol. Phys.* **2007**, *105*, 849–860. [[CrossRef](#)]
86. Charron, F.; Guo, B.; Zhang, K.; Morbi, Z.; Bernath, P. High-resolution infrared emission spectrum of CaF. *J. Mol. Spectrosc.* **1995**, *171*, 160–168. [[CrossRef](#)]
87. Liu, M.C.; Muntianu, A.; Zhang, K.Q.; Colarusso, P.; Bernath, P. Infrared emission spectrum of KF. *J. Mol. Spectrosc.* **1996**, *180*, 188–192. [[CrossRef](#)]
88. Muntianu, A.; Guo, B.; Bernath, P.F. High-resolution infrared emission spectrum of NaF. *J. Mol. Spectrosc.* **1996**, *176*, 274–279. [[CrossRef](#)]
89. Bauer, R.K.; Lew, H. Rotational constants and electric dipole moment of NaF. *Can. J. Phys.* **1963**, *41*, 1461–1469. [[CrossRef](#)]
90. Veazey, S.E.; Gordy, W. Millimeter-wave molecular-beam spectroscopy: Alkali fluorides. *Phys. Rev.* **1965**, *138*, A1303. [[CrossRef](#)]
91. Green, G.W.; Lew, H. Rotational spectrum of ³⁹KF by the molecular beam electric resonance method. *Can. J. Phys.* **1960**, *38*, 482–494. [[CrossRef](#)]
92. Dijkerman, H.; Flegel, W.; Gräff, G.; Mönter, B. Beiträge zum Stark-Effekt der Moleküle ²⁰⁵Tl¹⁹F und ³⁹K¹⁹F / Contributions to the Stark-Effect of the Molecules ²⁰⁵Tl¹⁹F and ³⁹K¹⁹F. *Z. Für Naturforschung A* **1972**, *27*, 100–110. [[CrossRef](#)]
93. Barber, B.; Zhang, K.; Guo, B.; Bernath, P. Vibration-rotation emission spectrum of MgF. *J. Mol. Spectrosc.* **1995**, *169*, 583–589. [[CrossRef](#)]
94. Le Roy, R.J. dPotFit: A computer program to fit diatomic molecule spectral data to potential energy functions. *J. Quant. Spectrosc. Radiat. Transf.* **2017**, *186*, 179–196. [[CrossRef](#)]
95. Shayesteh, A.; Bernath, P.F. Rotational analysis and deperturbation of the $A^2\Pi \rightarrow X^2\Sigma^+$ and $B'^2\Sigma^+ \rightarrow X^2\Sigma^+$ emission spectra of MgH. *J. Chem. Phys.* **2011**, *135*, 094308. [[CrossRef](#)]

96. Mostafanejad, M.; Shayesteh, A. Ab initio potential energy curves and transition dipole moments for the $X^2\Sigma^+$, $A^2\Pi$ and $B^2\Sigma^+$ states of MgH. *Chem. Phys. Lett.* **2012**, *551*, 13–18. [[CrossRef](#)]
97. Shayesteh, A.; Henderson, R.D.E.; Le Roy, R.J.; Bernath, P.F. Ground state potential energy curve and dissociation energy of MgH. *J. Phys. Chem. A* **2007**, *111*, 12495–12505. [[CrossRef](#)]
98. Yadin, B.; Vaness, T.; Conti, P.; Hill, C.; Yurchenko, S.N.; Tennyson, J. ExoMol Molecular line lists: I The rovibrational spectrum of BeH, MgH and CaH the $X^2\Sigma^+$ state. *Mon. Not. R. Astron. Soc.* **2012**, *425*, 34–43. [[CrossRef](#)]
99. Steimle, T.C.; Shirley, J.E.; Simard, B.; Vasseur, M.; Hackett, P. A laser spectroscopic study of gas-phase TiH. *J. Chem. Phys.* **1991**, *95*, 7179–7182. [[CrossRef](#)]
100. Launila, O.; Lindgren, B. Spectroscopy of TiH: Rotational analysis of the $^4\Gamma \rightarrow X^4\Phi(0,0)$ band at 530 nm. *J. Chem. Phys.* **1996**, *104*, 6418–6422. [[CrossRef](#)]
101. Andersson, N.; Balfour, W.J.; Bernath, P.F.; Lindgren, B.; Ram, R.S. Emission spectra of TiH and TiD near 938 nm. *J. Chem. Phys.* **2003**, *118*, 3543–3548. [[CrossRef](#)]
102. Andersson, N.; Balfour, W.J.; Lindgren, B. Rotational analysis of the $^4\Gamma - ^4\Phi$ spectrum of TiD. *J. Mol. Spectrosc.* **2003**, *217*, 298–299. [[CrossRef](#)]
103. Bauschlicher, C.W.; Ram, R.S.; Bernath, P.F.; Parsons, C.G.; Galehouse, D. The $A^6\Sigma^+ - X^6\Sigma^+$ transition of CrH, Einstein coefficients, and an improved description of the A state. *J. Chem. Phys.* **2001**, *115*, 1312–1318. [[CrossRef](#)]
104. Dulick, M.; Bauschlicher, C.W.; Burrows, A.; Sharp, C.M.; Ram, R.S.; Bernath, P. Line intensities and molecular opacities of the FeH $F^4\Delta - X^4\Delta$ transition. *Astrophys. J.* **2003**, *594*, 651–663. [[CrossRef](#)]
105. Phillips, J.G.; Davis, S.P.; Lindgren, B.; Balfour, W.J. The Near-Infrared Spectrum Of The FeH Molecule. *Astrophys. J. Suppl.* **1987**, *65*, 721–778. [[CrossRef](#)]
106. Curtis, M.C.; Sarre, P.J. High-resolution laser spectroscopy of the Swan system ($d^3\Pi_g - a^3\Pi_u$) of C_2 in an organic halide-alkali metal flame. *J. Mol. Spectrosc.* **1985**, *114*, 427–435. [[CrossRef](#)]
107. Suzuki, T.; Saito, S.; Hirota, E. Doppler-limited dye-laser excitation spectrum of the C_2 Swan band ($NU'-NU''=1-0$). *J. Mol. Spectrosc.* **1985**, *113*, 399–409. [[CrossRef](#)]
108. Prasad, C.V.V.; Bernath, P.F. Fourier transform spectroscopy of the Swan ($d^3\Pi_g - a^3\Pi_u$) system of the jet-cooled C_2 molecule. *Astrophys. J.* **1994**, *426*, 812–821. [[CrossRef](#)]
109. Tanabashi, A.; Amano, T. New identification of the visible bands of the C_2 Swan system. *J. Mol. Spectrosc.* **2002**, *215*, 285. [[CrossRef](#)]
110. Tanabashi, A.; Hirao, T.; Amano, T.; Bernath, P.F. The Swan system of C_2 : A global analysis of Fourier transform emission spectra. *Astrophys. J. Suppl.* **2007**, *169*, 472–484; Erratum: 2007 ApJS 170 261. [[CrossRef](#)]
111. Yurchenko, S.N.; Szabo, I.; Pyatenko, E.; Tennyson, J. ExoMol Molecular line lists XXXI: The spectrum of C_2 . *Mon. Not. R. Astron. Soc.* **2018**, *480*, 3397–3411. [[CrossRef](#)]
112. Furtenbacher, T.; Szabó, I.; Császár, A.G.; Bernath, P.F.; Yurchenko, S.N.; Tennyson, J. Experimental Energy Levels and Partition Function of the $^{12}C_2$ Molecule. *Astrophys. J. Suppl.* **2016**, *224*, 44. [[CrossRef](#)]
113. Ram, R.S.; Bernath, P.F. Fourier transform spectroscopy of the $A^2\Pi_i - X^2\Sigma^+$ system of CP. *J. Mol. Spectrosc.* **1987**, *122*, 282–292. [[CrossRef](#)]
114. Ram, R.S.; Tam, S.; Bernath, P.F. The $A^2\Pi_i - X^2\Sigma^+$ system of CP: Observation of new bands. *J. Mol. Spectrosc.* **1992**, *152*, 89–100. [[CrossRef](#)]
115. Saito, S.; Yamamoto, S.; Kawaguchi, K.; Ohishi, M.; Suzuki, H.; Ishikawa, S.I.; Kaifu, N. The microwave spectrum of the CP radical and related astronomical search. *Astrophys. J.* **1989**, *341*, 1114–1119. [[CrossRef](#)]
116. Klein, H.; Klisch, E.; Winnewisser, G.; Königshofen, A.; Hahn, J. CP's triple-bond strength experienced in its THz spectrum. *Z. Für Naturforschung A* **1999**, *54*, 187–190. [[CrossRef](#)]
117. de Brouckère, G.; Feller, D. Configuration interaction calculations on the state of CP and the-transition bands. Miscellaneous properties. *J. Phys. B At. Mol. Opt. Phys.* **1998**, *31*, 5053. [[CrossRef](#)]
118. Ram, R.S.; Wallace, L.; Bernath, P.F. High resolution emission spectroscopy of the $A^2\Pi - X^2\Sigma^+$ (red) system of $^{12}C^{14}N$. *J. Mol. Spectrosc.* **2010**, *263*, 82–88. [[CrossRef](#)]
119. Ram, R.S.; Davis, S.P.; Wallace, L.; Engleman, R.; Appadoo, D.R.T.; Bernath, P.F. Fourier transform emission spectroscopy of the $B^2\Sigma^+ - X^2\Sigma^+$ system of CN. *J. Mol. Spectrosc.* **2006**, *237*, 225–231. [[CrossRef](#)]
120. Davis, S.P.; Abrams, M.C.; Rao, M.L.P.; Brault, J.W. CN Vibration-Rotation Spectrum. *J. Opt. Soc. Am. B* **1991**, *8*, 198–200. [[CrossRef](#)]

121. Horka, V.; Civiš, S.; Spirko, V.; Kawaguchi, K. The infrared spectrum of CN in its ground electronic state. *Collect. Czech. Chem. Commun.* **2004**, *69*, 73–89. [[CrossRef](#)]
122. Ram, R.S.; Tereszchuk, K.; Gordon, I.E.; Walker, K.A.; Bernath, P.F. Fourier transform emission spectroscopy of the $E^2\Pi - X^2\Sigma^+$ transition of CaH and CaD. *J. Mol. Spectrosc.* **2011**, *266*, 86–91. [[CrossRef](#)]
123. Weck, P.F.; Stancil, P.C.; Kirby, K. Theoretical study of the rovibrationally resolved transitions of CaH. *J. Chem. Phys.* **2003**, *118*, 9997–10005. [[CrossRef](#)]
124. Furtenbacher, T.; Császár, A.G.; Tennyson, J. MARVEL: Measured active rotational-vibrational energy levels. *J. Mol. Spectrosc.* **2007**, *245*, 115–125. [[CrossRef](#)]
125. Alavi, S.F.; Shayesteh, A. Einstein A coefficients for rovibronic lines of the $A^2\Pi - X^2\Sigma^+$ and $B^2\Sigma^+ - X^2\Sigma^+$ transitions of CaH and CaD. *Mon. Not. R. Astron. Soc.* **2017**, *474*, 2–11. [[CrossRef](#)]
126. Boesch, A.; Reiners, A. Spectral line lists of a nitrogen gas discharge for wavelength calibration in the range 4500–11 000 cm^{-1} . *Astron. Astrophys.* **2015**, *582*, A43. [[CrossRef](#)]



© 2020 by the authors. Licensee MDPI, Basel, Switzerland. This article is an open access article distributed under the terms and conditions of the Creative Commons Attribution (CC BY) license (<http://creativecommons.org/licenses/by/4.0/>).